

#### 4. APPLICATION TO A BEAM-CONTROL REFLECTARRAY

In order to use this gain-enhancement technique for a beam-control reflectarray, it is necessary to determine the effects of the superstrate on the variations of the reflected phase. Using the waveguide approach (WGA) [6] and Ansoft's high-frequency structure simulator (HFSS) software, we have simulated the phase reflected by a multilayer reflectarray unit cell of dimensions  $17 \times 17 \text{ mm}^2$ . The basic radiating element is a rectangular slotted patch with a via connected to the ground plane (see Figure 3). It has the same characteristics as the element described in [5]. Figures 4(a) and 4(b) show the computed results for the reflection-coefficient magnitude and phase, respectively. These curves are plotted versus the via position  $X_p$  from the center of the patch, for different thicknesses of the superstrate  $t_3$ . These thicknesses are expressed in terms of wavelength  $\lambda_3$  in the superstrate medium ( $\lambda_3 = \lambda_0 / \sqrt{\epsilon_{r,3}}$  with  $\lambda_0$  the free-space wavelength at 10 GHz). The distance  $t_2$  between the patch and the superstrate is fixed to 14 mm, which is close to  $\lambda_0/2$ . The reflection coefficient is better than 0.985 across the entire range of the phase curve. Without the top-plate superstrate, the reflection coefficient is equal to unity. It can be seen that the variation of the reflected phase versus the position of the via  $X_p$  depends on the thickness of the superstrate. This dependence is particularly sensitive around the resonance frequency of the patch. However, by increasing the superstrate thickness, the relatively rapid phase transition leads to a faster change in the behavior of the resonance of the patch, followed by a decrease in bandwidth. Then, for this kind of reflectarray structure using a rectangular slotted patch with a via connected to ground plane, the thickness of the superstrate must be lower than a quarter-wavelength in order to achieve a practical operational bandwidth of the resulting reflectarray with gain enhancement and better phase range.

#### 5. CONCLUSION

In this paper, a substrate–superstrate method to enhance the gain of the microstrip reflected array has been presented. Large gains may be obtained at a given frequency by adjusting the distance  $t_2$  between the antenna patch and the superstrate. Using a dielectric superstrate of dielectric permittivity  $\epsilon_r = 10$ , a gain increase of 5 dB has been measured. The influence of the superstrate upon the radiation pattern and the reflected phase has also been measured and analysed.

#### REFERENCES

1. D.M. Pozar, D. Targonski, and H.D. Syrigos, Design of millimeter wave microstrip reflect arrays, *IEEE Trans Antennas Propagat* 45 (1997), 287–296.
2. K.M. Shum, Q. Xue, C.H. Chan, and K.M. Luk, Investigation of Microstrip Reflect array using a photonic bandgap structure, *Microwave Opt Technol Lett* 28 (2001), 114–116.
3. D.R. Jackson and N.G. Alexopoulos, Gain enhancement methods for printed antennas, *IEEE Trans Antennas Propagat* AP-33 (1985), 976–987.
4. X-H Shen, G.A. Vandenbosh, and A.R. Van de Capelle, Study of gain enhancement method, *IEEE Trans Antennas Propagat* 43 (1995), 227–231.
5. S.M. Meriah, E. Cambiaggio, F.T. Bendimerad, R. Staraj, and J.P. Damiano, Design of reflectarrays using slotted microstrip antennas with via connecting to ground plane, *Microwave Opt Technol Lett* 43 (2004), 368–370.
6. F.-C.E. Tsai and M.E. Bialkowski, An equivalent waveguide approach to designing of reflectarrays using variable size microstrip patches, *Microwave Opt Technol Lett* 34 (2002), 172–175.

© 2005 Wiley Periodicals, Inc.

## A TAPERED SMALL-SIZE EBG MICROSTRIP BANDSTOP FILTER DESIGN WITH TRIPLE EBG STRUCTURES

S. Y. Huang and Y. H. Lee

Integrated System Research Laboratory, S1-b2a-04  
School of Electrical and Electronics Engineering  
Nanyang Technology University  
50 Nanyang Avenue, Singapore 639798

Received 5 January 2005

**ABSTRACT:** A novel tapered small-size electromagnetic band-gap (S-EBG) microstrip filter structure is proposed and implemented. This structure is comprised of a main 1D microstrip EBG structure and two auxiliary EBG structures arranged in a compact configuration and Chebyshev distribution is adopted to eliminate ripples in the passband. It exhibits an ultra-wide stopband with high attenuation and excellent transmission in the passband, yet the circuit area remains small. © 2005 Wiley Periodicals, Inc. *Microwave Opt Technol Lett* 46: 154–158, 2005; Published online in Wiley InterScience (www.interscience.wiley.com). DOI 10.1002/mop.20929

**Key words:** EBG microstrip structures; microstrip bandstop filters; tapering techniques; Chebyshev distribution

#### 1. INTRODUCTION

Electromagnetic band-gap (EBG) structure has been a term widely accepted nowadays to name the artificial periodic structures that prohibit the propagation of electromagnetic waves at microwave or millimeter-wave frequencies. The original idea of the periodic structure (or crystal) was proposed at optical frequencies [1–3] and the structures were known as photonic band-gap (PBG) or photonic crystal (PC) structures. Analogous to crystals where periodic arrays of atoms produce band gaps in which the propagation of photons is prohibited, an artificial periodic structure is comprised of periodic macroscopic cells. These periodic structures are scalable and work in a wide frequency range in the electromagnetic spectrum. Due to their scalability, relevant research work has progressed in the microwave, millimeter-wave, and infrared [4] fields.

The unique feature of EBG structures is the existence of the band gap, in which electromagnetic waves are not allowed to propagate. It has been widely applied as the substrate of planar microwave circuits, such as patch antennas, to suppress the surface waves [5] and power amplifiers to reduce the harmonics [6]. The introduction of the planar EBG structure [7] in which periodic elements are etched in the ground plane simplifies the fabrication process of the periodic band-gap structure, while maintaining a similar control on the wave propagation in the structure to that of a 1D or 2D electromagnetic crystal (EC), where periodic rods are arranged in a host medium or columns are drilled through the substrate. The only trade-off with planar structures is that they are not able to realize a 3D EBG structure where the band gap exists in the entire 3D space. Nevertheless, planar EBG structures are highly compatible with microstrip-line circuits and make contributions to a number of high-performance compact microstrip-filter designs.

A microstrip line with an array of patches etched in the ground plane exhibits a prominent band gap in the direction along the conducting line [7]. Due to the high confinement of electromagnetic waves around the transmission line, a single column of periodically etched elements below the line is sufficient to obtain

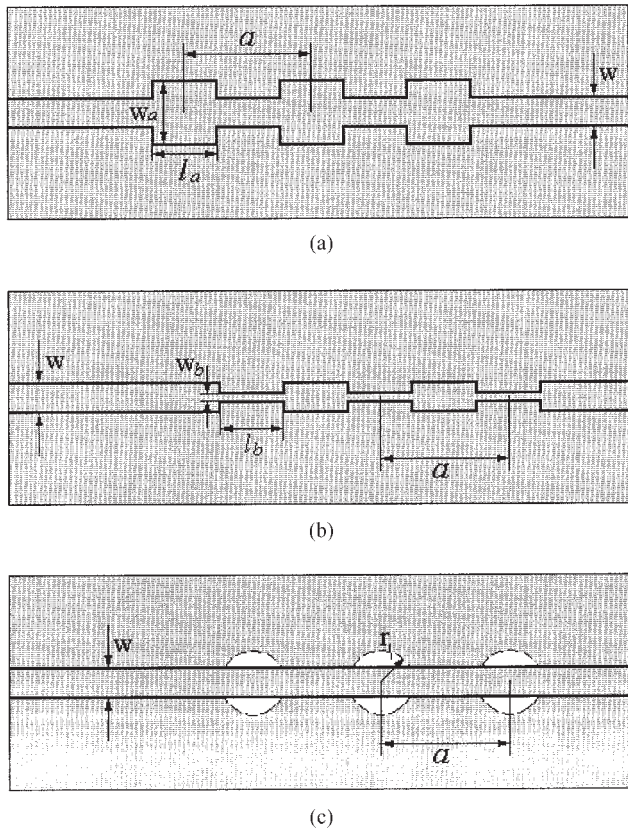


**Figure 1** Schematic of 1D planar EBG microstrip structures: (a) main EBG structure with rectangular patches inserted in the transmission line; (b) auxiliary EBG structure 1 with stepped impedance; (c) auxiliary EBG structure 2 with one column of circles etched in the ground plane

a band gap when the Bragg reflection condition is satisfied [8], which is the well known 1D EBG microstrip reflector.

A band gap can be obtained in the microstrip line when the geometry of the etched patch is changed or when the periodic elements are introduced in the microstrip line [9, 10]. The defected ground structure (DGS) has defects with a unique geometry and is able to exhibit an attenuation pole even with a single unit [11].

Several approaches have been taken to enhance the stopband performance of 1D planar microstrip EBG Bragg reflectors while maintaining a reasonable ripple level in the passband and keeping a small physical size. In [12], in order to create a high-performance bandstop filter that exhibits a wide stopband with high attenuation in a relatively small physical area, a meandering 1D EBG microstrip line was proposed. In [13], a compact EBG structure with a wide stopband was proposed by combining a 1D periodic DGS and a modulated microstrip line. This structure is able to introduce a significant increase in the bandwidth of the stopband while maintaining a small ripple level in the passband.

In this paper, a novel small-size EBG (S-EBG) microstrip structure with triple EBG structures is proposed. This newly developed EBG structure is based on a main EBG microstrip line with rectangular patches periodic inserted in the line [Fig. 1(a)]. It is superposed with two other auxiliary EBG structures [Figs. 1(b) and 1(c)] to enhance the reactance contrast in the EBG cell. This S-EBG microstrip structure achieves a significant increase in the bandwidth and attenuation of the stopband within a small circuit area (three EBG cells). The low-side-lobe array theory (Chebyshev distribution) is adopted to further tailor the ripple level in the passband and optimize the structure.

This proposed tapered S-EBG microstrip structure has a similar geometric configuration as that of the double-sided microstrip PBG filter [14], which combines a traditional microstrip lowpass filter on the top and an EBG perturbed ground plane at the bottom. However, the proposed structure has a different working principle from that of the structure in the literature. It is an EBG microstrip Bragg reflector whose design is restricted by the Bragg reflection condition. With the novel configuration, the proposed design achieves a great improvement of the stopband performance and a significant reduction in physical size, and demonstrates a new approach to eliminate passband ripples. The tapered S-EBG microstrip filter structure proposed in this paper is a high-performance compact EBG microstrip bandstop filter exhibiting excellent transmission and rejection characteristics.

## 2. SMALL-SIZE EBG MICROSTRIP BANDSTOP FILTER DESIGN

Figure 2 shows the schematics of the proposed small-size EBG (S-EBG) microstrip structure. For the three EBG structures in Figure 2, each structure has three elements arranged at a period of  $a$  and they satisfy the Bragg reflection condition.

As can be seen in the 3D schematic in Figure 2(a), the proposed structure has a modulated microstrip line on the top which is a combination of the main EBG structure and the auxiliary EBG structure 1 in Figures 1(a) and 1(b), respectively. The thin microstrip-line sections in the auxiliary EBG structure 1 were located between the inserted rectangular patches in order to enhance the variation of impedance. On the ground plane, there is another auxiliary EBG structure with etched circles [Fig. 1(c)] that are exactly below the thin line sections so as to further increase the inductance seen from the microstrip line. The dielectric material between the transmission line and the ground plane is Taconic with dielectric constant  $\epsilon_r$  of 2.43 and thickness  $h$  of 30 mils.

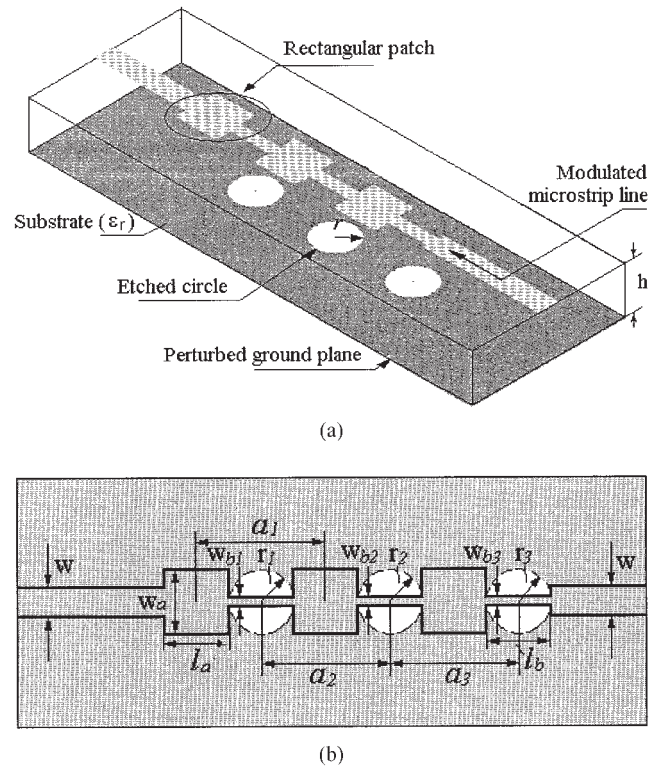


**Figure 2** Schematic of the proposed dual-plane small-size EBG (S-EBG) structure: (a) 3D view; (b) top view

Figure 2(b) shows the top view of the proposed structure. As can be seen in the figure, the centers of the two auxiliary EBG structure overlap and are located at the middle point between two centers of adjacent inserted patches. To operate in the X-band range, the center frequency of the main EBG structure [Fig. 1(a)] was set to be 10 GHz and the period of the structure  $a_1$  was determined to be 10.4 mm according to the Bragg reflection condition. Therefore, the periods of the two auxiliary EBG structures  $a_2$  and  $a_3$  were decided to both be 10.4 mm. The width of the microstrip line  $w$  was set to be 2.3 mm, corresponding to a characteristics impedance of  $50\Omega$  at 10 GHz. The length and width of the inserted rectangular patch in the microstrip line  $l_a$  and  $w_a$  were both fixed to 5 mm. Thus, the length  $l_b$  of the thin microstrip line section in auxiliary EBG structure 1 was determined to be 5.4 mm. Its width  $w_b$  was set to be 0.3 mm. The radius of the circle  $r$  in auxiliary EBG structure 2 was set to be 2.6 mm, thus avoiding any overlap between the etched circle and the inserted patch in the main EBG structure.

To eliminate the ripple due to the EBG periodicity in the proposed S-EBG structure, the Dolph-Tschebyscheff array (known as Chebyshev distribution) from the low-side-lobe array theory [15] was adopted to taper the dimension of EBG cells in the two auxiliary EBG structures. In our design, a three-element array with a major-to-minor lobe ratio of 25 dB was used for the

**TABLE 1 Performance of Microstrip EBG Structures**

EBG Structure	10-dB Bandwidth	Attenuation	Ripple Level	
			Lower	Higher
Main EBG structure	—	9.3dB	0.7dB	2.5dB
S-EBG	11.1GHz	39.3dB	2.3dB	7.0dB
Tapered S-EBG	10.2GHz	35.9dB	0.5dB	4.3dB

three-cell EBG structures in the proposed design. The normalized coefficients were determined as 0.729, 1, and 0.729. In auxiliary EBG structure 1, 1 corresponds to the cutting area of the center cell and the cutting area of the other two cells are tapered. Thus, both  $w_{b1}$  and  $w_{b3}$  were determined to be 0.8 mm. In auxiliary EBG structure 2, 1 corresponds to the area of the center circle. Therefore, the radius of the circle from left to right was determined to be 2.2, 2.6, and 2.2 mm, respectively.

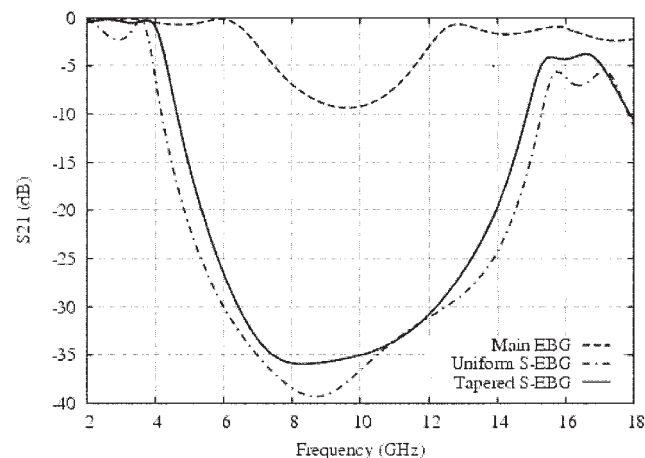
The simulations were conducted using a method of moments (MoM)-based software, Zeland IE3D™. Figure 3 compares the simulated  $S$ -parameters of the main EBG structure, the proposed S-EBG microstrip filter structure, and the optimized tapered S-EBG structure. As we can see from Figure 3(a), the main EBG structure exhibits an evident band gap at 10 GHz when patches are periodically inserted in the microstrip line. However, its performance is inferior in terms of the bandwidth and attenuation of the rejection band. The rejection performance of the main EBG structure has been dramatically improved by the introduction of two auxiliary EBG structures in the proposed structure in this paper. An ultrawide stopband with high attenuation can clearly be observed in the performance of the proposed S-EBG structure. With only three EBG cells, this proposed structure is able to obtain a 25-dB bandwidth of 7.4 GHz with a center frequency of 10 GHz. However, its ripple levels in both passbands become high when the stopband is enhanced. In the tapered S-EBG structure, the ripple level in the passband is significantly lowered. Although the bandwidth is reduced by 8.8% by adopting the tapering technique to the two auxiliary EBG structures, it is still much larger than that shown by the traditional EBG structure (such as the main EBG structure in this paper).

Table 1 shows the performance of these three structures in terms of the ripple level in the passband, the rejection bandwidth, and the attenuation. As compared to the main EBG microstrip structure, the tapered S-EBG microstrip filter structure proposed in this paper achieves a dramatic increase in the bandwidth of the stopband and a 286% increase in the attenuation, yet keeping a similar ripple level in the lower and high passbands.

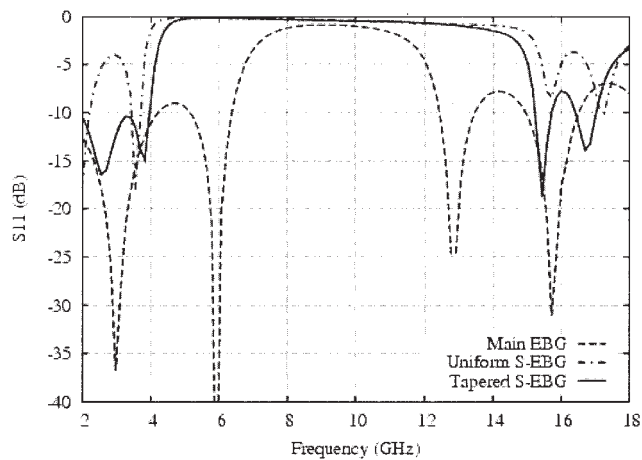
### 3. MEASURED RESULT

The proposed tapered S-EBG microstrip filter structure with a 44-mm-long transmission line was fabricated and tested. Figure 4 shows the photographs of the fabricated structure and Figure 5 shows the simulated and measured  $S$ -parameters. As can be seen from the measurement results, the proposed structure is able to achieve a 25-dB bandwidth of 6.3 GHz with a center frequency of about 10 GHz, attenuation of 36.1 dB, a ripple level of 0.8 dB in the lower passband, and a ripple level of 6.4 dB in the higher passband. Excellent agreement between the measurements and the simulation results has been obtained. The slight difference is possibly due to the lack of cell uniformity and material uniformity, and over etching.

The tapered S-EBG microstrip structure proposed in this paper is able to obtain excellent passband and stopband characteristics. Multilayer substrate or via holes are not required to fabricate this



(a)



(b)

**Figure 3** Simulated  $S$ -parameters of the dual-plane small-size EBG (S-EBG) structure and the two single-plane EBG structures: (a)  $S_{21}$ ; (b)  $S_{11}$

novel structure, thus favoring fabrication. This proposed structure demonstrates the advantages of ultrawide bandwidth, high attenuation, smooth passband, compact size, and an easy fabrication process. It can be easily applied to circuit applications requiring broadband-filtering functionality.

#### 4. CONCLUSION

The design and implementation of a novel tapered small-size EBG (S-EBG) microstrip bandstop filter have been presented. The proposed structure consists of a main EBG structure with rectangular patches periodically inserted in the microstrip line and two auxiliary EBG structures in order to enhance the reactance contrast in an EBG cell. With these three EBG structures in a unique configuration, the novel structure has an ultrawide stopband with high attenuation and a small physical size in both longitudinal and transversal dimensions. Its ripple level in the passband is well

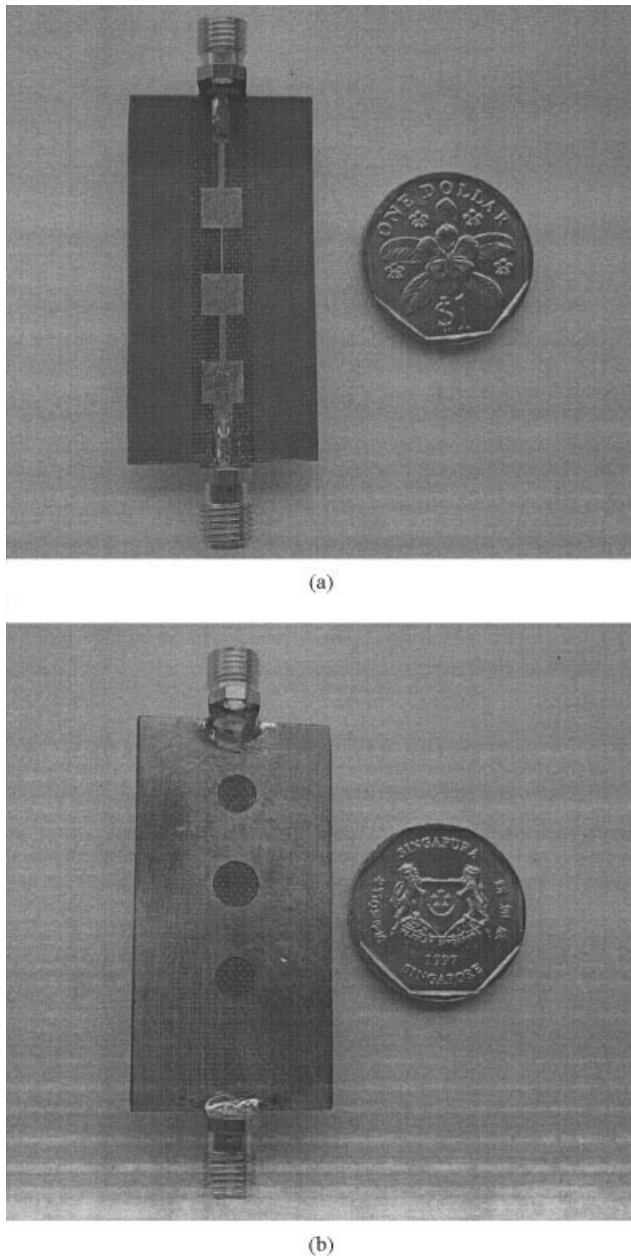


**Figure 4** Photographs of the fabricated dual-plane S-EBG structure: (a) front side; (b) back side

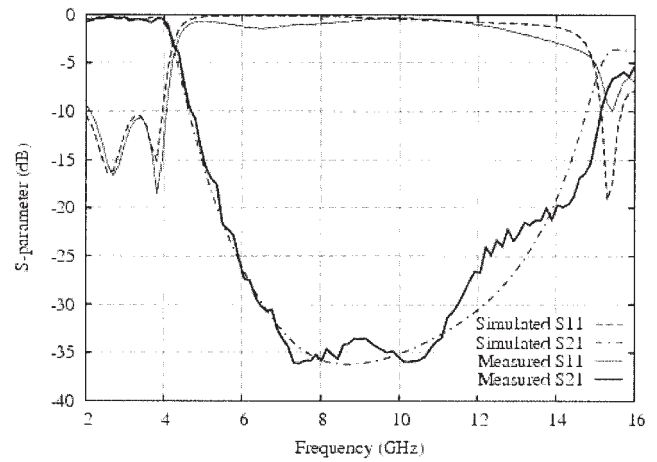


**Figure 5** Simulated and measured  $S$ -parameters of the fabricated dual-plane small-size EBG (S-EBG) structure

tailored by adopting the low-side-lobe array theory and, therefore, it exhibits an excellent transmission in the passband. This structure is easy to fabricate and is compatible with MMIC technology. The novel design of this structure enables it to achieve high performance as a bandstop filter with superior performance in the passband and stopband within a compact physical size. This unique EBG configuration provides an alternative approach, which can be taken to enhance the stopband of a 1D EBG microstrip structure. The structure proposed in this paper can be further employed in various applications for microwave circuits, such as the coupling suppression of two close microstrip lines and reflectors for the design of resonators.

#### REFERENCES

1. E. Yablonovitch, Inhibited spontaneous emission in solid state physics and electronics, *Phys Rev Lett* 58 (1987), 2059–2062.
2. S. John, Strong localization of photons in certain disordered dielectric superlattices, *Phys Rev Lett* 58 (1987), 2486–2489.
3. G. Kurizki and A.Z. Genack, Suppression of molecular interactions in periodic dielectric structures, *Phys Rev Lett* 61 (1988), 2269–2272.
4. E.R. Brown, Millimeter-wave applications of photonic crystals, *Wkshp Photonic Bandgap Structures*, Park City, 1992.
5. E.R. Brown, C.D. Parker, and E. Yablonovitch, Radiation properties of a planar antenna on a photonic-crystal substrate, *J Optical Soc Amer B* 10 (1993), 404–407.
6. V. Radisic, Y. Qian, and T. Itoh, Broadband power amplifier using dielectric photonic bandgap structure, *IEEE Microwave Guided Wave Lett* 8 (1998), 13–14.
7. V. Radisic, Y. Qian, R. Coccioli, and T. Itoh, Novel 2D photonic bandgap structure for microstrip lines, *IEEE Microwave Guided Wave Lett* 8 (1998), 69–71.
8. F. Falcone, T. Lopetegi, and M. Sorollah, 1D and 2D photonic bandgap microstrip structures, *Microwave Opt Technol Lett* 22 (1999), 411–412.
9. Q. Xue, K.M. Shum, and C.H. Chan, Novel 1D microstrip PBG cells, *IEEE Microwave Guided Wave Lett* 10 (2000), 403–405.
10. T. Lopetegi, M.A.G. Laso, J. Hernandez, M. Bacaicoa, D. Benito, M.J. Garde, M. Sorollah, and M. Guglielmi, New microstrip “wiggly-line” filters with spurious passband suppression, *IEEE Trans Microwave Theory Tech* 49 (2001), 1593–1598.
11. D. Ahn, J.S. Kim, Y. Qian, and T. Itoh, A design of the lowpass filter using the novel microstrip defected ground structure, *IEEE Trans Microwave Theory Tech* 49 (2001), 86–93.
12. F. Falcone, T. Lopetegi, M. Irisarri, M.A.G. Laso, M.J. Erro, and M. Sorollah, Compact photonic bandgap microstrip structures, *Microwave Opt Technol Lett* 23 (1999), 233–236.

13. J.Y. Kim and G.Y. Lee, Wideband and compact bandstop filter structure using double-plane superposition, *IEEE Microwave Wireless Compon Lett* 8 (1998), 69–71.
14. T. Akalin, M. Laso, E. Delos, T. Lopetegi, O. Vanbesien, M. Sorolla, and D. Lippens, High performance double-sided microstrip PBG filter, *Microwave Opt Technol Lett* 13 (2003), 279–280.
15. C. Balanis, *Antenna theory analysis and design*, Wiley, New York, 1997.

© 2005 Wiley Periodicals, Inc.

## SPECTRALLY ACCELERATED BICONJUGATE GRADIENT STABILIZED METHOD FOR SCATTERING FROM AND PROPAGATION OVER ELECTRICALLY LARGE INHOMOGENEOUS GEOMETRIES

Baris Babaoglu, Ayhan Altintas, and Vakur B. Ertürk

Department of Electrical and Electronics Engineering  
Bilkent University  
TR-06800, Bilkent Ankara, Turkey

Received 4 January 2005

**ABSTRACT:** Scattering from and propagation over rough-terrain profiles, as well as reentrant surfaces are investigated using an integral equation (IE)-based spectrally accelerated biconjugate gradient stabilized (SA-BiCGSTAB) method, with a storage requirement and a computational cost of  $O(N)$  per iteration, where  $N$  is the surface unknowns in the discretized IE. Numerical results in the form of current and path loss are presented and compared with previously published as well as measured results in order to assess the accuracy and efficiency of this method. © 2005 Wiley Periodicals, Inc. *Microwave Opt Technol Lett* 46: 158–162, 2005; Published online in Wiley InterScience (www.interscience.wiley.com). DOI 10.1002/mop.20930

**Key words:** biconjugate gradient stabilized method; electromagnetic rough-surface scattering; method of moments; spectral acceleration; propagation over terrain

### 1. INTRODUCTION

Accurate analysis of electromagnetic-field strengths and propagation over rough-surface profiles has great importance for military and commercial applications such as frequency-channel planning, coverage area estimation, and so forth. Therefore, various solution methods have been proposed. Majority of them are propagation-prediction models such as the Okumura, Hata, and ITU-370 approaches [1–3], which depend on empirical formulas obtained via statistical analysis, yielding general scattering or diffraction properties. More accurate predictions can be obtained using integral equation (IE)-based methods solved via the method of moments (MoM). However, they suffer from the storage and the computational-cost requirements when applied to electrically large geometries, even though using an iterative method can alleviate the computational cost to some extent. Therefore, the spectral acceleration (SA) algorithm was developed in [4] for slightly rough surfaces and modified in [5] to handle very undulating geometries, which accelerated the stationary forward-backward method (FBM) [6] and decreased both the computational cost and memory requirements to  $O(N)$ . However, the spectrally accelerated FBM (SA-FBM) fails when the geometry of interest is a multivalued one, such as a reentrant surface of a ship, due to the nature of the FBM [7]. To overcome this problem, the spectrally accelerated

generalized forward-backward method (SA-GFBM) and the multiblock generalized forward-backward method (MBGFBM) have been proposed in [8] and [9], respectively. It should be noted that in [8], although the overall computational cost is  $O(N)$ , the SA-GFBM becomes computationally expensive when the reentrant region becomes electrically large, whereas in [9], the proposed MBGFBM has an overall computational cost of  $O(N^2)$  and is claimed to be reduced to  $O(N)$  when combined with the SA algorithm. Naturally, the implementation of SA-GFBM and MBGFBM is scatterer specific, which is undesirable for the development of general purpose codes.

In this paper, electrically large rough-terrain profiles as well as reentrant geometries have been examined using the nonstationary iterative spectrally accelerated biconjugate gradient stabilized method (SA-BiCGSTAB) with a storage requirement and a computational cost of  $O(N)$ , where the SA principles given in [5] are used. Although the SA algorithm is valid for ordered surfaces (which becomes problematic for a reentrant geometry), such a geometry remains inside the strong field region in the SA-BiCGSTAB method, and requires a computational complexity of  $O(N_s^2)$  (with  $N_s$  the number of unknowns for the strong region) as opposed to  $O(N_s^3)$ , reported in [8]. Hence, in addition to its accuracy and robustness due to the nonstationary nature of BiCGSTAB method, the SA-BiCGSTAB method becomes more efficient than the SA-GFBM. Moreover, the  $O(N_s^2)$  operational count for the strong region can be improved by using the fast-multipole method (FMM) in conjunction with the BiCGSTAB method [10]. Consequently, inherent robustness of a nonstationary technique (BiCGSTAB) has been merged with the SA algorithm in order to investigate electrically large arbitrary profiles efficiently and accurately. Such a hybrid method whose convergence characteristics is independent of the surface geometry, is very suitable for general scattering problems.

The paper is organized as follows: in section 2, the geometry and the formulation of the problem are given with a brief explanation of the spectrally accelerated BiCGSTAB method. In section 3, numerical results composed of current distributions and path losses are given and compared with the measurements and previously published results in order to assess the accuracy and efficiency of the method. An  $e^{j\omega t}$  time convention is employed and suppressed throughout the paper.  $\omega$ ,  $k$ , and  $\lambda$  are the angular frequency, wave number, and wavelength of free space, respectively.

### 2. FORMULATION

An arbitrary-terrain profile with no variation along the transverse direction of the propagating field, as in [4–9, 11–14] is depicted in Figure 1. The electromagnetic fields characterized by  $\mathbf{E}^i$  and  $\mathbf{H}^i$  are incident upon the surface. The terrain profile is modeled to be an imperfect conductor (with permeability  $\mu$  and permittivity  $\epsilon$ ) and analyzed using an impedance boundary condition (IBC) [15] to be able to investigate more general situations.

#### 2.1. IE and MoM Formulation

An IE is formed by applying IBCs on the surface of the scatterer, and the EFIE for a TM wave can be written as

$$-E_y^i = -\eta_s J_y(\rho) - \frac{\omega\mu}{4} \int_C J_y(\rho') H_0^{(2)}(k|\rho - \rho'|) d\rho' - j \frac{k\eta_s}{4} \int_C J_y(\rho') \hat{n} \cdot \hat{\rho} H_1^{(2)}(k|\rho - \rho'|) d\rho'. \quad (1)$$